Date of publication xxxx 00, 0000, date of current version xxxx 00, 0000.
Digital Object Identifier XX.XXXX/YYY.20XX.ZZZZZZZ

A Modular Reconfigurable Battery Architecture with an Adaptive Real-Time Control Strategy for Optimal Capacity Utilization

GHADA BEN DEBBA[1], ALI AMAMOU[2],(Member, IEEE), SOUSSO KELOUWANI[3], (Senior Member, IEEE), and NAIMA SEHLI,[1]

[1]Department of Electrical Engineering, University of Quebec at Trois-Rivieres, Trois-Rivieres, QC, G9A 5H7, Canada.
[2]National Integrated Smart Manufacturing Center, Drummondville, QC, J2C 0R5, Canada.
[3]Department of Mechanical Engineering, University of Quebec at Trois-Rivieres, Trois-Rivieres, QC, G9A 5H7, Canada.

Corresponding author: GHADA BEN DEBBA (e-mail: ghada.ben.debba@uqtr.ca).

ABSTRACT Addressing the challenges of cell inconsistency in battery systems, a key factor affecting performance, dynamic reconfigurable batteries (DRBs) have emerged as a promising solution in recent research, ensuring better cell balancing and optimal energy use. However, existing designs often face trade-offs between control complexity, switching flexibility, and operational reliability, limiting their practicality for large-scale applications. To overcome these limitations, this study proposes a novel balancing strategy based on a modified modular architecture with flexible module-level switching. This design relies on a dual-layer control framework that simultaneously manages inter- and intra-module state of charge (SOC) equalization with reduced coordination overhead. A Genetic Algorithm-based approach is used for optimal switching control, enhanced by a Feedforward Neural Network (FNN) to predict SOC deviation, enabling efficient and reliable real-time balancing. Experimental validation on a lab-scale prototype and Hardware-in-the-Loop (HIL) simulations demonstrates the system's ability to improve battery capacity utilization and extend operating time by approximately 17% and 18%, respectively, compared with conventional system. Further testing on a large-scale pack with 320 cells demonstrates up to 40 minutes of additional autonomy over a fixed architecture, underlining the practical potential of the proposed method for real-world applications.

INDEX TERMS Dynamic reconfigurable battery, cell balancing, Feedforward Neural Network (FNN), genetic algorithm, real-time control, vehicle autonomy.

I. INTRODUCTION

There have been significant advances in battery technology over the past decade focused on improving energy storage performance, minimizing resource usage, and enhancing overall sustainability [1]. These advances have paved the way for a whole range of applications, from consumer electronics to renewable energy systems and electric vehicles. However, as global demand for energy continues to grow and diversify, existing battery systems face significant challenges related to system performance degradation and capacity inconsistency between individual cells. These inconsistencies arise from several factors such as manufacturing tolerances [2], stochastic nature of battery aging processes [3], and environmental conditions [4]. Such disparities become more pronounced over time, especially in systems where cells remain permanently interconnected, leading to a progressive decline in overall performance [5, 6].

To mitigate cell inconsistencies, traditional balancing techniques have evolved from simple energy dissipation methods to more advanced energy redistribution systems [7, 8]. Early passive balancing approaches equalized cell voltages by dissipating excess energy from overcharged cells through resistive elements [9]. While simple and low-cost, this method is inherently inefficient, as the dissipated energy is lost as heat. To improve energy utilization, active balancing techniques were developed, enabling energy transfer between cells using capacitive, inductive, or converter-based circuits [10]. Although these methods achieve faster and more efficient balancing, they introduce higher circuit complexity, increased cost, and potential reliability concerns due to the additional components involved [11].

Faced with these challenges, dynamic reconfigurable bat-

teries (DRBs) have sparked a surge of interest in recent research [12–14]. Instead of relying on dedicated energy transfer circuits with fixed cell topologies, DRB systems leverage high-speed power electronic switches to create a flexible battery network. This reconfigurability enables the system to respond dynamically to changes in cell behavior and operational conditions [15–17], thereby improving fault tolerance [18, 19], enhancing energy management [20–22], and extending battery lifespan [23–25]. Various battery designs with sophisticated control methodologies have been explored in existing research, however, finding an appropriate compromise between flexibility and reliability remains a major challenge [13].

At the pack design level, various architectures have been proposed with different numbers of switches, ranging from one to six switches per cell or module [26]. Low-switch designs, such as one or two per cell or module, are often favored for their simplicity in control and low hardware overhead [27–29]. However, this simplicity comes at the cost of limited reconfiguration flexibility, which restricts energy optimization and SOC balancing capabilities. Moreover, these architectures often rely on additional components, such as redundant cells or DC/DC converters to compensate their limited reconfiguration options [30]. Conversely, architectures incorporating more than three switches per cell offer greater reconfiguration flexibility [31], enabling advanced equalization processes and fine-grained control of energy distribution, particularly under significant SOC disparities [32]. This improved flexibility, however, increases management complexity, wiring density, computational burden, and overall system cost. A comparative summary of these design trade-offs is provided in Table 1.

Regarding control strategies, they are generally classified into three categories: Rule-Based, Optimization-Based and Data-Driven approaches. Rule-based approaches relies on predefined heuristics, which can be easier to interpret and require fewer computing resources [33, 34]. However, their effectiveness is limited as they often focus on prioritizing the use of the most powerful cells without considering the long-term system performance. Optimization-based approaches, aim to find the optimal cell configuration throughout the operating cycle by formulating and solving mathematical optimization problems. These strategies can be implemented using online methods such as Model Predictive Control (MPC), which operate in real time, predicting future system states and iteratively solving optimization problems to determine the best control actions [35], or offline methods such as Dynamic Programming (DP) [36] which pre-compute optimal policies for efficient implementation during operation. However, these approaches require significant computational resources and highly accurate system models, while also facing scalability challenges for large-scale batteries. Moreover, offline methods rely on the assumption of a predetermined load profile which is not practical in real applications. Data-driven approaches such as Deep Reinforcement Learning (DRL) [37, 38] and Q-Learning [39, 40], leverage machine learning to adaptively optimize control strategies, excelling in complex, non-linear systems but requiring extensive training data and careful validation to ensure reliability [31].

Despite their advantages over fixed configurations, existing DRB strategies still encounter several challenges, particularly when it comes to real-world applications. One of the main challenges is the complexity inherent in large-scale batteries. Indeed, several studies have focused on extending the battery's energy supply by managing each cell configuration individually [36–41]. However, as the number of cells and switches grows, control complexity emerges and system management will be difficult to handle, requiring more sophisticated control algorithms and hardware, which may impact overall performance and reliability. Safety concerns are also a major challenge. These include the risk of load isolation during real-time reconfiguration, as well as the potential risk of control switching malfunctioning in complex configurations, resulting in short-circuit problems [42]. Additionally, managing the voltage difference between the load and the battery when bypassing lower-charged cells presents another problem. To address this, additional components such as DC/DC converters have been used, to maintain output voltage within the operating range [43, 44]. Alternatively, some strategies rely on redundant cells to handle this issue [29, 33]. However, these components increase energy losses and system costs, adding further constraints to the practicality of the system. Finally, most existing research on DRB strategies is limited to small-scale battery systems, with a lack of experimental validation on large-scale setups. This gap raises concerns about the scalability and practicality of these methods in real-world, large-scale applications. Within this context, this paper addresses the aforementioned gaps and introduces a new reconfigurable battery architecture with a dual-scale equalization strategy. The main contributions of this study are outlined as follows:

- A modular reconfigurable architecture is proposed, featuring three switches per cell and one switch per module. This design enhances reconfiguration flexibility by enabling seamless transitions between parallel and series configurations, ensuring effective balancing without the need for additional components.
- An adaptive real-time control framework is developed, combining Genetic Algorithms (GA) for optimal switching with a Feedforward Neural Network (FNN) for SOC deviation prediction. This approach addresses real-time control complexity by simultaneously managing intra- and inter-module equalization through a unified switch command, maintaining both safety and performance under dynamic load conditions.
- Finally, scalability is demonstrated through comprehensive testing on a large-scale system comprising 320 cells. The seamless adaptation to larger systems high-

TABLE 1. State of the art comparative analysis.

Topology		Flexibility	Cost (Extra Hardware)	Control Complexity	Balancing Efficiency
Conventional System [10, 45, 46]	Passive Balancing [9]	Low	Low (resistors)	Low	Low
	Active Balancing [47, 48]	Low	Moderate (Capacitors / Inductors / Transformers)	Moderate	Moderate
DRB System	Less than 3 switch/cell [27, 29, 49, 50]	Low	Moderate (Redundant cells / DC-DC converter)	Moderate	Moderate
	More than 3 switch/cell [31, 32, 51–53]	High	High (many switches, wiring)	High (cell-level control)	High
	Proposed Architecture 3 switch/cell and 1 switch/module	Moderate	Moderate	Moderate (module-level control)	High

lights the method's capability to manage complex configurations effectively, bridging the gap between theoretical research and industrial applications.

Based on these contributions, the proposed design aims to achieve a balanced trade-off between flexibility, complexity, and energy efficiency, as illustrated in Table 1. The remainder of this paper is organized as follows. The proposed DRB system is described in Section II. Section III presents the control strategy framework. Section IV presents the simulation results and discussions. Finally, conclusions are drawn in Section V.

II. SYSTEM MODELING

The main objective of reconfigurable battery systems is to optimize capacity utilization through a dynamic adjustment of the cell's connectivity for a better charge equilibrium. This configuration depends on both circuit architecture and the associated control strategy. A detailed description of the proposed design and reconfigurable strategy is presented in this section.

A. BATTERY PACK PROPOSED ARCHITECTURE

A battery pack is generally composed of several units, each consisting of a series-parallel configuration of cells. Managing a large number of cells within a single unit poses significant challenges. A modular architecture offers a practical solution to reduce management complexity while enhancing scalability. As illustrated in Fig.1, the proposed design considers a battery unit as a set of modules connected in parallel. A module can be connected or bypassed through a controllable switch S_{M_i}. Each module, M_i, consists of n number of cells, where each cell c_i is equipped with three switches, $\{s_1, s_2, s_3\}$, enabling flexible transitions between series and parallel configurations. This modular structure localizes the flexibility required for reconfiguration within each module, enabling simultaneous intra- and inter-module balancing with simplified control coordination. The equalization mechanism is detailed in Section II-C.

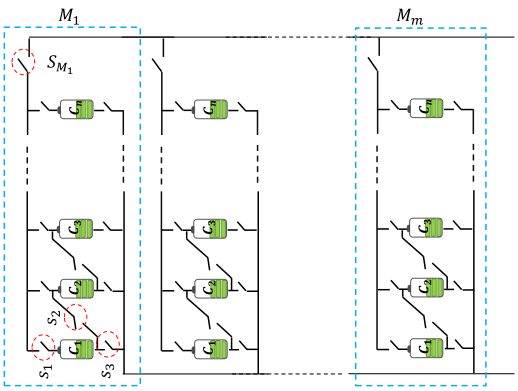

FIGURE 1. DRB system proposed architecture.

According to Kirchhoff's laws, the unit's output current and voltage are presented as follows:

$$I_{\text{unit}}(t) = \sum_{j=1}^{m} S_j I_j(t) \tag{1a}$$

$$V_{\text{unit}}(t) = \sum_{i=1}^{n} v_i(t) \tag{1b}$$

where I_j represents the output current from the j^{th} module, S_j is a binary indicator reflecting the module's switch status (S_j=1 if the module is connected, 0 otherwise), m is the number of modules, and n the number of cells within each module. v_i denotes the voltage of the i^{th} cell, given cells are connected in series in normal operation, contributing to the total voltage V_{unit}. This configuration can be further extended to build a large-scale battery pack with several parallel units, making it suitable for real-life applications and adaptable to meet a variety of operational demands.

B. SINGLE CELL MODEL

An equivalent circuit model (ECM) is developed to capture the dynamic behaviour of each cell as shown in Fig.2. Thevenin model is used in our study as it offers a balanced trade-off between accuracy and computational simplicity [54]. While higher-order models may better capture transient effects and diffusion dynamics, they impose significantly higher computational demands, which can be impractical for embedded control implementations in large-scale battery systems [55, 56]. The first-order ECM supports these constraints while providing sufficient fidelity for control decisions [48, 57].

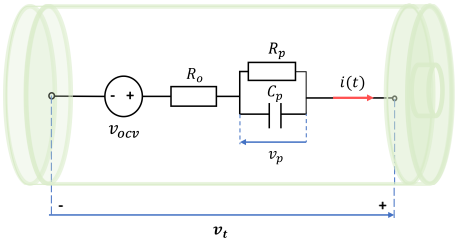

FIGURE 2. Thevenin equivalent circuit model.

The mathematical model of the ECM is established as follows:

$$v_t(t) = v_{ocv}(soc(t)) - R_o i(t) - v_p(t) \tag{2}$$

where v_{ocv} is the open circuit voltage, R_o is the internal resistance and v_p is the polarization voltage, which is defined as:

$$\dot{v_p}(t) = -\frac{1}{R_p C_p} v_p(t) + \frac{1}{C_p} i(t) \tag{3}$$

where R_p and C_p are the polarization resistance and capacitance. The cell's SOC during normal operation, is determined using Coulomb Counting method [58], as follow:

$$soc(t) = soc_{t_0} - \frac{1}{3600} \int_{t_0}^{t} \frac{i(t)}{Q} dt \tag{4}$$

where soc_{t_0} and Q are a cell's initial SOC and capacity respectively. An SOC–OCV mapping is used to provide an accurate estimation of the initial SOC and maintains consistent Coulomb-counting tracking throughout operation [59, 60].

C. RECONFIGURABLE STRATEGY

Maximizing the usable capacity of the battery pack requires that all cells reach a comparable state of charge by the end of operation. In this regard, the control strategy addresses two primary challenges: (1) the SOC deviation between parallel modules (inter-module imbalance), and (2) the SOC deviation between cells within each module (intra-module imbalance). Effective balancing therefore requires mechanisms that operate at both levels. Different equalization strategies have been proposed with modular reconfigurable architecture. One-switch-per-module configurations allow simple inter-module balancing [27], but they lack the capability to resolve SOC imbalance within modules. Two-switch-per-cell designs can support intra-module control, but often require redundant cells or DC/DC converters to maintain voltage compatibility, which increases system cost and complexity [43]. Recent dual-layer or hierarchical strategies manage intra- and inter-module balancing separately through multi-stage control loops or sorting algorithms [41, 49]. While effective, these approaches introduce coordination delays and control overhead, which complicate real-time operation. To effectively handle these issues, a simplified dual-layer equalization strategy is proposed that manages both intra- and inter-module imbalance using a single-step control command. This strategy operates as follows.

1) Intra-Equalization Layer:

At this level, cell balancing within individual modules is achieved by temporarily isolating a given module and reconfiguring their cell arrangement from series to parallel as shown in the Fig.3. Meanwhile, the remaining cells in other modules continue to operate under standard conditions, ensuring system resilience and uninterrupted power delivery.

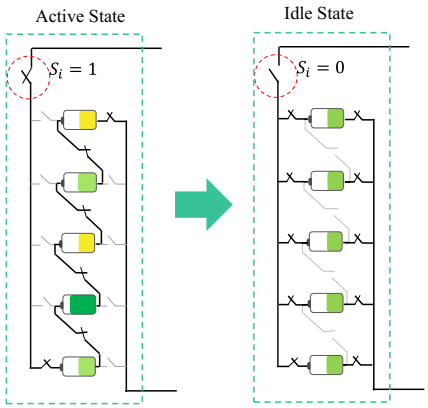

FIGURE 3. Intra-Module Equalization process.

This configuration promotes an even redistribution of energy between cells, enabling spontaneous equalization without the need of additional components [61]. Fig.4 illustrates simulation results for three lithium cells, each with a capacity of 2.5Ah, connected in parallel with different SOC values.

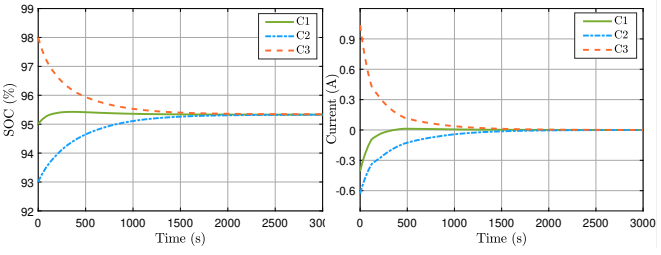

(a) (b)

FIGURE 4. Simulation results of 3 parallel connected cells in idle mode: (a) cell's SOC and (b) current.

As shown in Fig.4, the SOC difference between the 3 cells tends to decrease as energy is redistributed between them, and the equilibrium current tends towards zero. Unlike existing DRB strategies that balance cells during operation by selecting higher-charged cells and bypassing lower ones, the proposed approach performs balancing during the idle phase through direct energy exchange among cells. However, a long period of idle time may be required to reach equilibrium depending on cell behavior and divergence levels, which may affect system efficiency as the other modules remain in operation. Thus, an additional equalization layer is required to deal with this issue.

2) Inter-Equalization Layer

This layer focuses on harmonizing charge between modules throughout the battery system for consistent energy production. Modules with reduced capacity or significant SOC deviation are dynamically isolated. This selective isolation allows internal balance to be restored and reduces the deviation between modules. More than one module can be disconnected at any given time step, according to the load demands requirements, C_{rate} effect and the inner-module divergence levels.

The integrated control approach enables simultaneous management of the intra- and inter-module equalization process. By issuing a single control action at the module level, the system not only initiates intra-module balancing during idle phases but also influences the inter-module SOC dynamics through selective load redistribution. This unified mechanism reduces control overhead and enhances the effectiveness of the balancing process across the entire pack. Therefore, a sophisticated optimization control strategy is needed to deal with this dual-layer equalization strategy.

III. PROPOSED CONTROL FRAMEWORK

This section presents the proposed control framework, as illustrated in Fig. 5, providing a detailed formulation of the optimization problem and the methodologies employed to solve it.

A. OPTIMIZATION PROBLEM FORMULATION

In order to improve the system control efficiency, a multi-criteria optimization approach is used to find a compromise between several criteria:

- Minimize the SOC deviation between cells within individual modules: Intra-Equalization.
- Minimize the SOC disparities between modules to ensure consistent energy output : Inter-Equalization.
- Meeting load requirement: Optimize the number of active modules to increase system availability for load demand.

To address these objectives, a detailed formulation is described below:

1) State Space:

Given a battery unit with N cells organized into m parallel module, where each module is an array of n cells, $n = N/m$. At any given time step k the average SOC for each module can be represented as a vector:

$$\mathrm{SOC}_{\mathrm{avg}}(k) = \begin{bmatrix}\mathrm{SOC}_1(k) & \dots & \mathrm{SOC}_{m-1}(k) & \mathrm{SOC}_m(k)\end{bmatrix}^T$$

where $\mathrm{SOC_i}(k)$ represents the average SOC of the cells within module i, reflecting the module's capacity status :

$$\mathrm{SOC}_i(t) = \frac{1}{n}\sum_{j=1}^{n} soc_j^i(t) \tag{5}$$

Similarly, the standard deviation of SOC within each module is given by:

$$\sigma(k) = \begin{bmatrix}\sigma_1(k) & \dots & \sigma_{m-1}(k) & \sigma_m(k)\end{bmatrix}^T$$

where σ_i denotes the SOC standard deviation of module i at the time step k, indicating the uniformity of charge distribution between cells. It is calculated using the following equation:

$$\sigma_i(k) = \sqrt{\frac{\sum_{j=1}^{n}(soc_j^i(k) - SOC_i(k))^2}{n-1}} \tag{6}$$

where soc_j^i is the state of charge of cell j in module i, calculated using (4).

The state variable can be defined as a vector $\mathrm{X}(k) = \begin{bmatrix}\sigma_{\mathrm{ext}}(k) & \sigma_{\mathrm{int}}(k) & I_d(k)\end{bmatrix}^T$ where:

- $\sigma_{\mathrm{ext}}(k)$: Represents the external deviation, specifically the deviation of the SOC between modules at time step k (inter-module deviation), as described in (7):

$$\sigma_{ext}(k) = \sqrt{\frac{\sum_{i=1}^{m}(\mathrm{SOC}_i(k) - \overline{\mathrm{SOC}}(k))^2}{m-1}} \tag{7}$$

  where $\overline{\mathrm{SOC}}$ is the average SOC of the entire unit.

- $\sigma_{\mathrm{int}}(k)$: Denotes the internal deviation within the stack, i.e., the SOC deviation within each module at time step k (intra-module deviation). It is defined as the average standard deviation of the σ vector using (8):

$$\sigma_{int}(k) = mean(\sigma) = \frac{1}{m}\sum_{i=1}^{m}\sigma_i(k) \tag{8}$$

- $I_d(k)$: Represents the total delivered current from the entire unit at time step k, calculated as follow:

$$I_d(k) = \sum_{i=1}^{m} u_i(k)\cdot I_n \tag{9}$$

  where I_n is the nominal discharge current of a module and u_i is the switch state, to capture the number of active modules at time step k, $i = 1, \dots, m$.

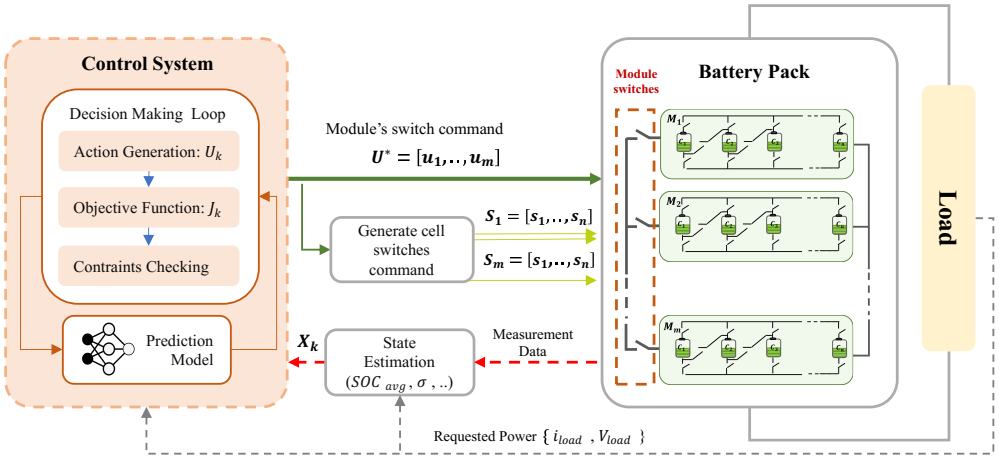

FIGURE 5. Overview of the DRB control process.

2) Decision Variables:

The control variable can be presented as a binary vector $U(k) = \begin{bmatrix} u_1(k) & \dots & u_{m-1}(k) & u_m(k) \end{bmatrix}^T$ where each element reflects the module connection status:

$$u_i(k) = \begin{cases} 1 & \text{if module } i \text{ is active} \\ 0 & \text{otherwise} \end{cases}$$

The switch command of cells within each module is defined also as a binary vector $S_i = [s_1, \dots, s_n]$, where s_j is the command of 3 switches related to cell j in module i. The cells switching command is associated with the connection status decision of the corresponding module. An active state mode, u_i =1, results in a series connection command, while an idle state mode results in either a parallel connection command or a bypassing command (where all cells in the module will be disconnected), depending on system requirements.

3) Cost Function:

The cost function quantifies the trade-offs between different criteria over a given prediction time horizon. It is expressed in (10), where the objective is to minimize the cost J with respect to the control input sequence U:

$$\min_U J = \min_U \sum_{k=0}^{T-1} \|X(k) - X_R(k)\|_\alpha^2 + \|U(k)\|_\beta^2 \quad (10)$$

Subject to:

- System's dynamics:

$$X(k+1) = f(X(k), U(k)) \quad (11)$$

- Constraints:

$$0 \leq soc_j^i \leq 1 \quad (12a)$$

$$I_{min} \leq I_i \leq I_{max} \quad (12b)$$

$$\sum_{i=1}^{m} u_i \cdot I_i \geq I_{load} \quad (12c)$$

where $\|a\|_M^2 = a^T M a$ denotes the weighted quadratic norm and T is the optimization time windows. $X_R(k) = \begin{bmatrix} \sigma_{ext_R}(k) & \sigma_{int_R}(k) & I_R(k) \end{bmatrix}^T$ is the reference state variable at time step k, where σ_{ext_R} and σ_{int_R} are the reference SOC inter- and intra-deviation, respectively. I_R is the reference current requested from the load at time step k. $\alpha = [\alpha_1, \alpha_2, \alpha_3]$ represents the relative weight vector, with $\sum_{i=1}^{3} \alpha_i = 1$, and β is a penalty factor that discourages excessive module switching, promoting system longevity and operational efficiency.

The system's dynamic function is a non linear function that may be approximated in two ways depending on the module's operating mode:

- In the **normal state**, when the module is connected to the load and the internal cells are configured in series, f is evaluated using the mathematical cell model presented in Section II-B, which is based on Coulomb Counting for SOC estimation.

- In the **equilibrium state**, the module is disconnected from the load and its internal cells are switched from series to parallel to enable energy redistribution as explained in Section II-C. During this phase, the average SOC of the module remains relatively unchanged, but the SOC values of individual cells change due to redistribution currents. This intra-module equalization process makes traditional model-based estimation approaches challenging, as they do not accurately capture the stochastic nature of redistribution currents and their effect on SOC dynamics. For this reason, a lightweight Feedforward Neural Network is employed to predict the short-term evolution of SOC deviation during the equilibrium phase, enabling more accurate decision-making within the optimization strategy. Further details are provided in the following section.

B. FEEDFORWORD NEURAL NETWORK PREDICTION MODEL

Various approaches have been developed in literature for SOC estimation, focusing mainly on cells during charge/discharge cycles [62, 63]. However, accurately predicting SOC behavior in parallel-connected cells during idle states remains a challenge. Conventional equivalent circuit models are not well-suited to capture the stochastic SOC variations that arise within parallel-connected groups, primarily due to differences in internal resistance, self-discharge rates, and capacity imbalance. To overcome this problem, the proposed strategy involves predicting the overall SOC deviation within each module, rather than each cell individually. This module-level prediction significantly reduces computational complexity by limiting the number of prediction targets while directly supporting the intra-module equalization process in the control strategy.

Within this context, a stochastic modeling approach is needed to capture the randomness and variability inherent in cell behavior. While recent machine learning models have shown promise for improving SOC estimation under complex conditions [64, 65], they often come with high computational demands and long training times. A Feedforward Neural Network (FNN) provides a lightweight yet effective solution due to its computational efficiency and fast inference, making it well-suited for real-time control applications [66, 67]. A detailed description of the network architecture, data preparation process, and evaluation metrics are presented as follows:

- **Model Architecture:** A regression model is used to predict the expected change in SOC deviation for a given module containing n parallel-connected cells. Two key features are considered as inputs: the average SOC and the current SOC deviation of the module, calculated respectively in equations (5) and (6). The incorporation of the average SOC as a feature is important due to the non-linear behavior of battery cells, where the evolution of variance differs according to SOC ranges. The network structure includes an input layer with these two features, one hidden layer with a sigmoid activation function, and a single-neuron output layer that provides the updated SOC deviation after a defined equilibration interval.

- **Data Preparation:** The dataset is generated using various simulation scenarios of modules with parallel-connected cells with different initial SOC distributions. Each scenario incorporates different discharging currents ranging from 0.5C to 2C to reflect realistic operating conditions. Data samples are recorded at fixed time intervals corresponding the time at which a module transitioned from active to idle state, capturing the evolution of SOC deviations. For each sample, the average SOC, the current deviation, and the updated deviation are computed and stored. An overview of the data generation pipeline and its integration with the FNN model is illustrated in Fig.6. Specific details, such as cell characteristics and the number of cells per module, are described in Section IV, based on each case study.

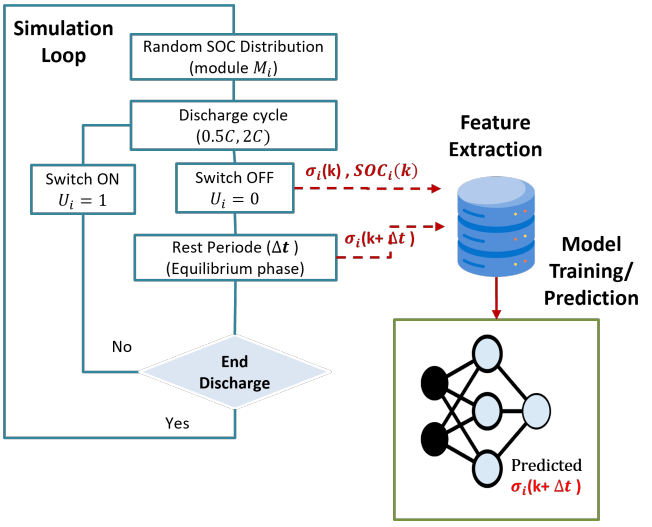

FIGURE 6. Workflow for database generation and integration with the FNN predictive model.

- **Performance Evaluation Metrics:** The performance of the model was evaluated by partitioning the dataset into training and testing subsets. The primary metrics used to measure the model's prediction accuracy were Mean Absolute Error (MAE) and Root Mean Square Error (RMSE):

$$\text{MAE} = \frac{1}{n}\sum_{i=1}^{n}|y_i - \hat{y}_i| \tag{13}$$

$$\text{RMSE} = \sqrt{\frac{1}{n}\sum_{i=1}^{n}(y_i - \hat{y}_i)^2} \tag{14}$$

  where n is the number of samples, y_i is the actual value, and $\hat{y}_i$ is the predicted value from the model.

The generated model is then integrated within the control strategy for the decision making process.

C. GA-BASED APPROACH FOR SWITCHING CONTROL

The optimization challenges within the DRB system arise from the combinatorial complexity of optimizing over discrete variable sets, represented by binary switch states, combined with the nonlinear dependencies inherent in the system's dynamics. Thus, the problem is classified as a mixed integer nonlinear programming (MINLP) problem. To effectively manage the complexity of the MINLP problem, a genetic algorithm (GA) approach is utilized. This method is particularly well-suited for non-linear problems involving binary decision variables [68], and is effectively applied in energy management systems to enhance performance and efficiency through complex optimization task [69, 70].

The working process of GA, as described in Algorithm 1, consists of iteratively exploring potential solutions within a given population, where each individual represents a possible switch configuration. This process incorporates the dynamic model and the fitness function described in (10) to evaluate each configuration. Selection mechanisms prioritize individuals according to their fitness score, promoting the generation of new solutions from well-adapted configurations through crossover and mutation. This evolutionary approach allows the GA to adeptly navigate the solution space, assessing each configuration's efficacy in meeting predefined performance criteria to generate the optimal switching control command U*.

Algorithm 1 GA-Based Optimization control stratrgy

Input: SOC values, Load demand
Output: Optimal switch configuration U^*

```
Initialize population with random switch configurations
Evaluate fitness of each individual: Cost Function J
for each generation do
    Select parents using tournament selection
    Create offspring via crossover
    Apply mutation to introduce variations
    Evaluate fitness of new individuals
    Replace least fit individuals with new offspring to maintain population size
    Check for termination criteria:
        - Performance criteria achieved
        - Maximum generations reached
        - No fitness improvement observed
end for
```

Managing N/n modules instead of N individual cells significantly reduces the search space from $O(2^N)$ to $O(2^{N/n})$, lowering the computational burden while preserving balancing effectiveness. To further improve efficiency and enable real-time execution, additional enhancements are integrated into the optimization process:

- Search Space Optimization: By incorporating the constraint (12c), the number of feasible solutions will be limited, ensuring that operational requirements are met while accelerating the optimization process.
- Early Stopping Mechanism: The algorithm terminates if no significant improvement is observed over multiple generations, conserving computational resources and avoiding unnecessary computations.
- Parameter Fine-Tuning: GA parameters, including population size, crossover rate, and mutation rate, are carefully optimized to balance exploration and exploitation, ensuring a thorough yet computationally efficient solution search.

Through these modifications, the proposed control strategy remains computationally efficient, scalable, and reliable while achieving optimal balancing and enhanced energy management.

IV. RESULTS AND DISCUSSION

This section presents a comprehensive evaluation of the proposed system through a comparative study, validation on a lab-scale prototype, and testing on a Hardware-in-the-Loop (HIL) system under dynamic driving cycles. Throughout these studies, A123 LiFePO4 cells with a nominal voltage of 3.3 V and a capacity of 2.3 Ah are used. The dynamic characteristics for the cell model are obtained from the manufacturer's datasheet of the A123 ANR26650 LiFePO4 cell, where the variation of OCV, R_0, R_1, and τ_1 with SOC under different operating temperatures is presented in Fig.7.

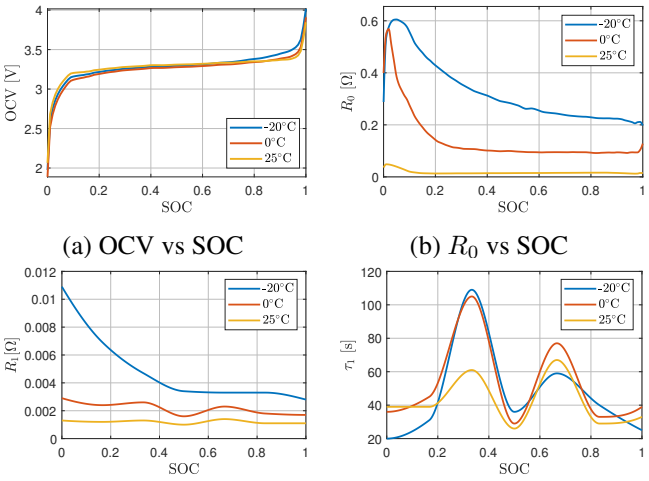

(a) OCV vs SOC (b) R_0 vs SOC

(c) R_1 vs SOC (d) τ_1 vs SOC

FIGURE 7. Battery cell dynamics modeled from manufacturers' datasheet of A123 LiFePO cell.

To simulate real-world inconsistency between cells, a random SOC distribution with a mean of 85% and a deviation of 7.5% is applied. Finally, the lower SOC threshold is set at 10% to ensure cell safety.

A. FNN MODEL PERFORMANCE ANALYSIS

The Feedforward Neural Network model is integrated into the GA-based control strategy to predict SOC deviations, providing critical input for the optimization process. Built using TensorFlow library, the model adheres to the architecture detailed in Section III-B. The initial training dataset was generated by simulating three parallel cells per module, corresponding to the configuration used in the first two case studies. These simulations included varying SOC distributions and discharging current. The evolution of the SOC deviation was recorded for each scenario with a sampling period of 1 s, in accordance with the control strategy time step. The performance of the FNN model is demonstrated through a detailed analysis of the mean square error (MSE) trend over 185 epochs, presented in Fig.8. The model reaches its best validation performance at epoch 185 with mean absolute error (MAE) and root mean square error (RMSE) of 1.8e-03 and 4e-03 respectively, demonstrating its convergence and reliability across different datasets.

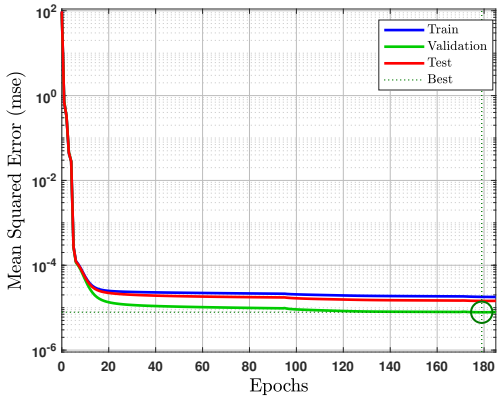

FIGURE 8. MSE result of the FNN model.

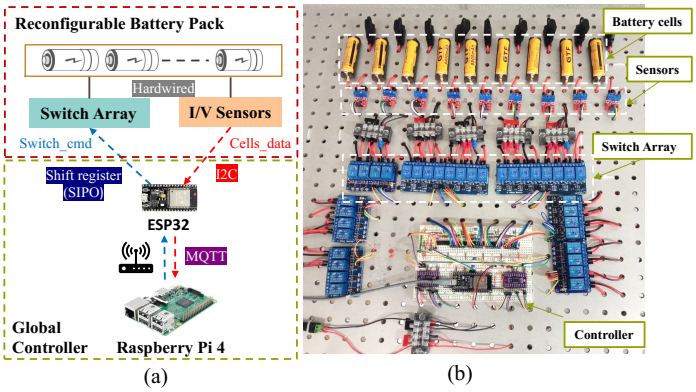

FIGURE 9. Lab-scale prototype of 9 cells: (a) device connection and communication, (b) device implementation.

To address larger configurations, an additional dataset was generated for modules comprising 16 cells, tailored to the scalable use case. This dataset incorporated enhanced diversity in initial SOC distributions to reflect the complexities of larger setups. The resulting model demonstrated similarly high performance, achieving RMSE of 1.7e-02 and MAE of 1.2e-02, ensuring its applicability to larger configurations without compromising prediction accuracy. In real-world applications, the predictive model is established once for the defined module configuration, enabling efficient and seamless integration into the control framework across different system scales.

B. DRB STRATEGY VALIDATION WITH A LAB-SCALE PROTOTYPE

To validate the effectiveness of the proposed DRB strategy, we compare it with an existing 4-switch architecture, known as the JPL architecture, which is widely recognized in the literature for its flexibility in cell management [36, 71]. The JPL design relies on full cell exploration through a cell-skipping strategy to reduce SOC deviation by dynamically adjusting the series-parallel cells configuration at each time step. The comparative analysis is conducted using a lab-scale prototype, presented in Fig.9. A detailed description of the experimental setup and results evaluation is provided in the following subsections.

1) Prototype Description:

The lab-scale prototype is built with 9 LiFePO4 cells, relay switches with a conductance resistance of 40 $m\Omega$ and INA226 sensors for current and voltage measurements with an accuracy of approximately ±0.5%. The Battery Management System (BMS) controller comprises an ESP32 microcontroller, which handles data acquisition from sensors via an I2C multiplexer and sends switching commands to relays through shift registers. A Raspberry Pi serves as the master controller, estimating the SOCs and executing the DRB algorithm. Communication between these controllers is established wirelessly using the MQTT protocol, ensuring seamless operation and data transfer. A programmable DC Load is used to set the discharging current.

2) Comparative Performance Analysis:

In this case study, we conduct the experimental test on three distinct systems: conventional system with a fixed architecture (3S3P), JPL architecture (from literature), named DRB system 1, and the proposed GA-based control architecture, named DRB system 2. All systems are initialized with the same random SOC distribution and subjected to a constant load current of 2.3A (1C). The experimental results are summarized in Fig.10 and Table 2. The performance of each DRB system compared to the conventional system are evaluated using the following metrics:

- Energy efficiency: Represents the ratio of the energy delivered to the load to the rated energy of the battery pack, describe as follow:

$$\eta_{energy}(\%) = \frac{E_{\text{load}}}{E_{\text{init}}} \times 100 \tag{15}$$

where E_{init} denotes the theoretical maximum energy stored in the battery pack, and E_{load} corresponds to the total energy delivered to the load over the entire discharge cycle. Given that reconfigurable batteries rely primarily on power switches to enable flexible configurations, the internal resistance of these switches can introduce measurable conduction losses, particularly under high current flow. These losses can be quantified as:

$$E_{\text{loss}} = \sum_{k=0}^{H} \sum_{i=1}^{N_s} R_{\text{on}} \cdot I_i^2(k) \cdot \Delta t \tag{16}$$

where N_s is the numbers of switches, I is the current flowing through the switch, Δt is the time step duration and H is the total number of discrete time steps. The energy delivered to the load is then computed as:

$$E_{\text{load}} = E_{\text{tot}} - E_{\text{loss}} \tag{17}$$

where E_{tot} is the total extracted energy at the end of the discharge cycle, taking into account internal losses due to cell resistances.

- Operating time: This metric quantifies the relative improvement in operating duration achieved by the DRB architecture relative to the conventional system. It is defined as:

$$T_{op}\,(\%) = \frac{T_{\text{DRB}} - T_{\text{Conv}}}{T_{\text{Conv}}} \times 100 \tag{18}$$

  where T_{DRB} and T_{Conv} represent the operating time of each system, captured at the end of the operating cycle, where SOC lower threshold is reached.
- Cells SOC consistency: Evaluates the SOC deviation across all cells at the end of the discharge cycle using the following expression:

$$\sigma_f\,(\%) = \sqrt{\frac{1}{N}\sum_{i=1}^{N}\left(\text{SOC}_i - \overline{\text{SOC}}\right)^2} \tag{19}$$

  where N is the total number of cells.

These metrics will be considered for the rest of the evaluations, to highlight the substantial improvements achieved by the DRB system compared to the conventional system.

The experimental results highlight the potential of both DRB System 1 and DRB System 2 in significantly reducing cell divergence throughout the discharge cycle, as illustrated in Fig. 10(b) and (c). These deviations, prominent in the conventional system (Fig. 10(a)), lead to early cut-off to avoid over-discharge, leaving a considerable portion of the battery capacity unused. In contrast, both reconfigurable strategies effectively mitigate these issues, ensuring more uniform cell discharge and achieving higher energy efficiency. Table 2 presents a quantitative comparison of performance metrics, demonstrating that both DRB systems deliver similar improvements over the conventional system. These strategies enhance operational time by approximately 19.3% and delivered energy by 19%, while reducing the final SOC deviation to near-zero values, confirming their efficacy in achieving optimal energy management

While DRB System 1, based on a 4-switch per cell architecture, enables faster SOC equalization, its reliance on cell-level exploration significantly increases computational complexity, ranging from $O(N)$ for simpler clustering-based methods to $O(2^N)$ when sophisticated exploration is required to evaluate all possible configurations. This results in higher management costs, potential risks of load isolation or misconfiguration, and poor scalability for large battery systems. Meanwhile, the proposed DRB System, adopts a modular approach, managing N/n modules instead of individual cells. Its dual-scale equalization strategy handles SOC balancing at both inter- and intra-module levels with a simultaneous switch command. The control complexity is significantly reduced through heuristic search using GA, lowering the computational burden while maintaining effective energy management. While it takes slightly longer to reach equilibrium, its reduced complexity, enhanced safety, and scalability make it a practical and cost-effective solution. For instance, with a 9-cell setup, DRB System 1 records an average execution time of 2.6 ms per iteration, while the proposed DRB System 2 achieves a faster execution time of 0.81 ms under the same conditions. This performance gap becomes increasingly critical as system size grows, directly affecting the feasibility of real-time optimization in large-scale applications.

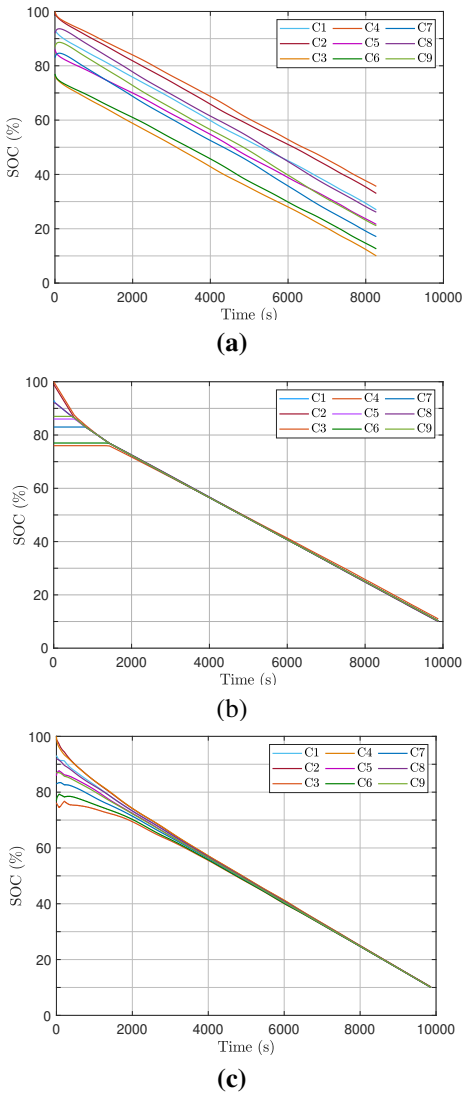

FIGURE 10. Experimental results: (a) cell SOCs with convectional system. (b) cell SOCs with DRB system 1. (c) cell SOCs with proposed DRB system 2.

C. PERFORMANCE EVALUATION ON HIL SYSTEM WITH DYNAMIC DRIVING CYCLE

To enable extensive testing under scalable and dynamic conditions, the proposed control strategy is deployed on a Hardware-in-the-Loop (HIL) system. While the lab-scale prototype is effective for demonstrating real-world feasibility, it is limited in terms of scalability, flexibility, and reproducibility for a wide range of scenarios. The HIL platform offers a safe, high-fidelity environment to evaluate the DRB strategy under diverse load profiles and system configura-

TABLE 2. Comparative study experiment results under constant current.

	E_{init} (Wh)	E_{load} (Wh)	η_{energy} (%)	T_{op}(h)	$\sigma_f(\%)$	Improvement (Energy)	Improvement (Time)	Average Execution Time per step (ms)
Conventional System	68.3	48.05	70.3	2h17min	6.9	-	-	-
JPL architecture (DRB system 1)	68.3	57.44	84.1	2h46min	0.1	19.6 %	19.4 %	2.6 ms
Proposed System (DRB system 2)	68.3	57.12	83.6	2h44min	0.08	18.9 %	19.3 %	0.81 ms

tions that would be difficult or time-consuming to replicate experimentally.

1) *HIL System setup:*

The proposed setup includes an OPAL-RT OP4510 simulator, a host laptop, and a Raspberry Pi microcontroller, as shown in Fig.11. An Ethernet-based UDP/IP communication protocol is used to ensures real-time data transmission, between the OPAL-RT simulator and the Raspberry Pi.

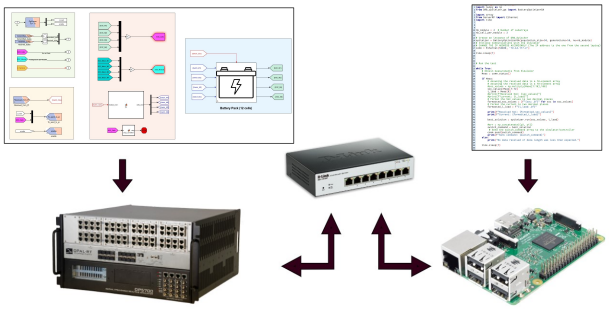

FIGURE 11. RTLab and Raspberry Pi UDP/IP communication model

The system emulates the proposed DRB architecture, modeled in MATLAB/Simulink, compiled into C code, and executed on the OPAL-RT for real-time operation. For battery cell modeling, a data-driven table-based model in MATLAB/Simulink [72] is used. This model is able to capture the dynamic charge-discharge behavior of lithium-ion cells accurately based on data provided in manufacturers' datasheets. The Raspberry Pi serves as the global controller to manage the tasks of BMS. It processes the data received from the OPAL-RT model, runs the GA-based optimization algorithm, and send the optimal switch command. To ensure a balance between responsiveness and effective equalization, the control time step is set to one second, assuming manageable load demand variations during this interval. We suppose that the load demand variation remain within a manageable range during this period. Additionally, a user interface console on the host laptop allows for data collection and visualization. The OPAL-RT simulator operates with a time step of 10^{-2}, ensuring high simulation accuracy. Before scaling up the configuration and applying dynamic load profiles, the proposed strategy was validated on the HIL system using the same 9-cell lab-scale prototype setup. The results showed good agreement with experimental outcomes, with an RMSE of approximately 3%. This variation is primarily attributed to switching delays, measurement inaccuracies and experimental conditions. Given this close alignment, the remainder of the study is carried out using the HIL system.

2) *HIL System results:*

In this case study, we consider a small battery pack comprising 12 LiFePO4 cells arranged in a 3S4P configuration. Since this reconfigurable battery is intended for vehicle applications, a WLTC (class 2) driving cycle is selected as a reference for generating discharge current profile. Regeneration is not considered, so there is no charging current. The calculated current is scaled down to meet system requirement as shown in Fig.12. This driving cycle is replicated multiple times to ensure full battery discharge within the test period.

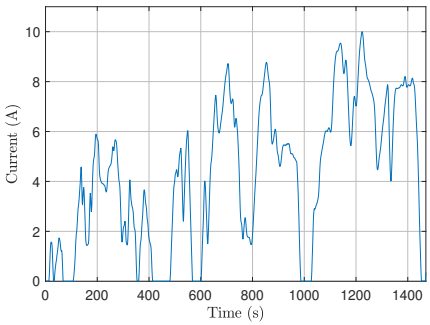

FIGURE 12. Load Current Profile (WLTC).

We conducted the same simulation tests with a conventional battery system under identical initial conditions and the same driving cycle. The duration of cycle is around 2 hours. The HIL system simulation results for both systems are presented in Fig.13, F and Table 3.

According to the HIL system results, we can clearly see in the conventional system, the divergence in voltage and SOC levels between cells throughout the discharge process, as shown in Fig.13(a) and (c). Meanwhile the difference in capacity between the cells decreases gradually with the proposed system, Fig.13(b) and (d), resulting in a 17% and 18% of improvement in term of capacity utilization rate and operating time respectively compared with the conventional system. This strategy effectively maintains the output voltage of the entire system within a range of approximately ±5% tolerance around the nominal output voltage of $9.9V$, as

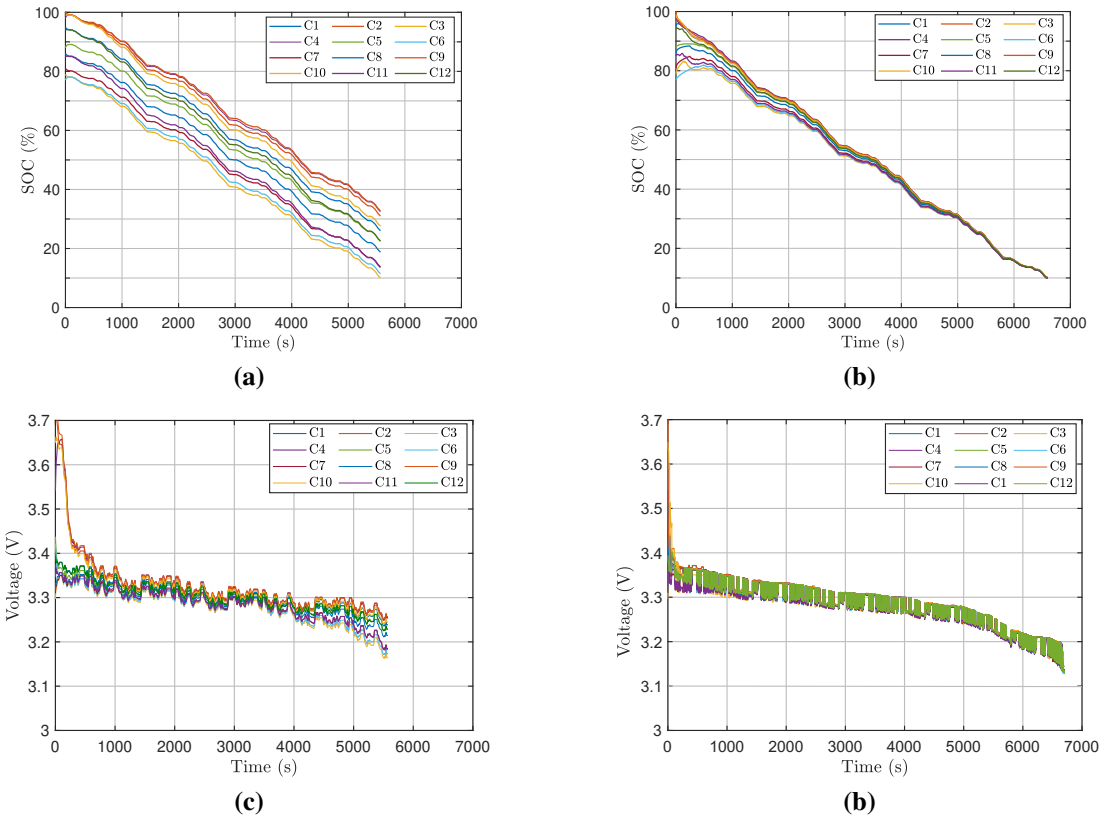

FIGURE 13. HIL simulation results: cell SOC with (a) conventional and (b) proposed DRB system. Cell voltages with (c) conventional and (d) proposed DRB system.

TABLE 3. DRB system performance analysis under WLTC (class 2) driven cycle.

	E_{init} (Wh)	E_{load} (Wh)	η_{energy} (%)	T_{op}(s)	σ_f(%)	Improvement (Energy)	Improvement (Time)
Conventional System	86.8	62	71.5	5568	7.16	-	-
JPL architecture	86.8	72.8	83.8	6579	0.11	17.4 %	18 %
Proposed System	86.8	73.2	84.5	6581	0.09	17.7 %	18.2 %

shown in Fig.14. This is achieved by ensuring that a sufficient number of high-charged modules remain connected to the load during reconfiguration, thus protecting the load from sudden interruptions.

Simulation results demonstrate the effective operation of the proposed GA-based control strategy. By ensuring seamless coordination between intra- and inter-module equalization layers, the approach effectively mitigates imbalance and enhances capacity utilization. Compared to the 4-switch architecture, the proposed strategy yields slightly improved performance under dynamic load conditions. This can be attributed to its ability to re-balance cells even while they are disconnected from the load, rather than skipping them. As a result, the SOC deviation is significantly reduced from 7.16% to 0.09% by the end of the discharge cycle.

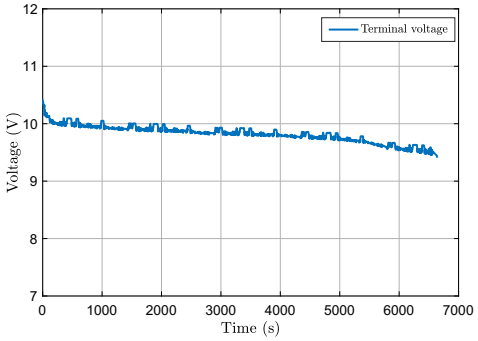

FIGURE 14. DRB system terminal voltage.

To strengthen the robustness assessment, a Monte Carlo analysis was conducted under the three WLTC driving-cycle classes (classes 1–3), which primarily differ in their

power demand dynamics and therefore span a wide range of operating conditions [73]. Each profile was evaluated over 30 randomized initial SOC distributions. The resulting histograms in Fig.15 summarize the average operating time and energy utilization rate for the conventional architecture, DRB System 1, and the proposed DRB System 2, including error bars that reflect variability across tests results.

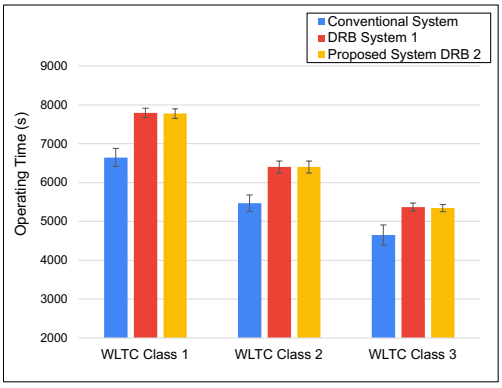

(a)

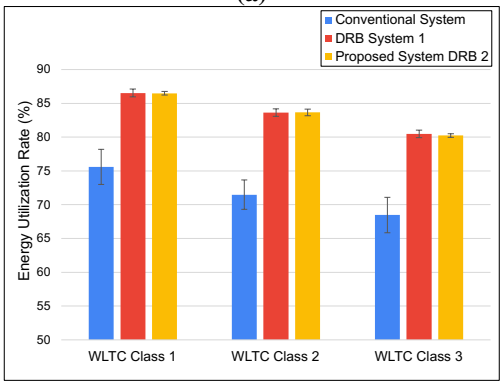

(b)

FIGURE 15. Monte-Carlo simulation results: (a) operating time and (b) energy utilization rate under three different driven cycles.

The proposed DRB system consistently demonstrates superior performance compared to the conventional architecture, with improvements in both operational autonomy and usable energy under low-demand (class 1) and high-demand (class 3) conditions. These results closely align with those achieved by DRB system 1, but with significantly lower complexity and improved security, particularly under dynamic driving conditions where the constraint of maintaining a minimum number of active modules is enforced.

D. SCALABILITY ANALYSIS AND VALIDATION

To emulate real-world conditions, this case study investigates a scalable battery pack modeled on an industrial vehicle battery, namely an autonomous forklift (AF), which is used in our lab in collaboration with an industrial partner [74]. The battery pack comprises three parallel units, each with a nominal voltage of 51.7 V and a capacity of 50 Ah. For this study, we focus on one unit configured with 320 cells in a 16S20P arrangement to meet specific operational

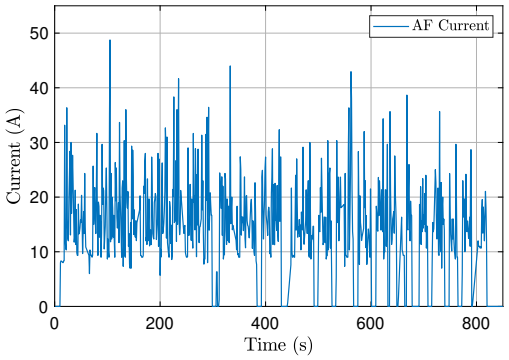

FIGURE 16. AF current profile during one mission.

requirements.The scalability of the proposed DRB strategy was validated using two load profiles: the WLTC driven cycle, previously used but scaled up to match the battery unit requirements, and a driving cycle based on real data recorded during an AF mission, as shown in Fig.16. The AF current profile was scaled down by a factor of three to reflect the usage of a single unit rather than the entire battery pack and replicated multiple times to creating a total duration of approximately three hours. This approach allowed for a detailed evaluation of battery performance and durability over prolonged operational periods. To enhance the speed and efficiency of data processing, the Raspberry Pi controller was replaced by a more powerful computing setup: a computer equipped with an Intel(R) Core(TM) i5-1035G1 CPU running at 2.50 GHz and 8GB of RAM. This upgrade significantly improved execution times, allowing for more complex computations and faster data handling during the simulation. Finally, a random distribution of the initial SOC was performed on the 320 cells, with a mean of 85% and a deviation of 7.5%. The same tests were also applied to a conventional battery with a fixed architecture. The HIL experiment results for both systems are presented in Fig.17 and Table 4.

As shown in Fig.17(a), the SOC inconsistency between cells in a conventional system persists until the end of the discharge cycle, highlighting the prevalence of module and cell imbalance in large-scale battery systems. Meanwhile, within the reconfigurable strategy, there is a significant improvement in the gap between cells as shown in Fig.17(b). It can be seen also, in Fig.17(c), that equalization between modules is achieved within 322 s by reconfigurable control, showing its effectiveness in balancing speed. These results demonstrates how effectively inter- and intra-module equalization mechanisms are applied, ensuring better SOC balance even in large-scale applications while maintaining terminal voltage within safe operational ranges, as shown in Fig.18. Furthermore, efficient SOC distribution management significantly enhances capacity utilization and extends operating time, achieving an additional 20 min under the WLTC driving cycle and up to 40 min with the AF mission cycle, as detailed in Table

TABLE 4. Performance analyses of proposed strategy with a large-scale battery system.

	E_{init} (Wh)	E_{load} (Wh)	η_{energy} (%)	T_{op} (h)	Improvement (Energy)	Improvement (Time)	Average Execution Time per step (s)
	WLTC driven cycle (class 2)						
Conventional System	2425.5	1673.4	69	1h21min	-	-	
JBL architecture	2425.5	2066	85.1	1h43min	24%	27%	1.81s
Proposed System	2425.5	2049.5	84.5	1h41min	23%	24%	0.31s
	AF mission profile						
Conventional System	2425.5	1649.34	68	2h18min	-	-	
JBL architecture	2425.5	2080.5	86	3h	26.4%	30%	1.83s
Proposed System	2425.5	2061.67	85	2h58min	25%	29%	0.32s

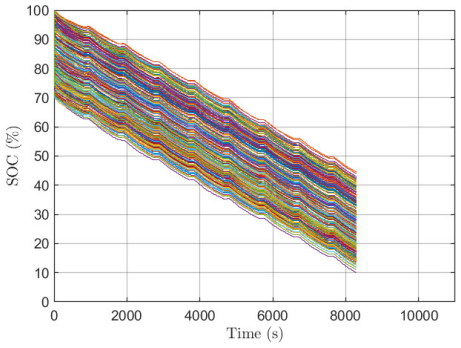

(a)

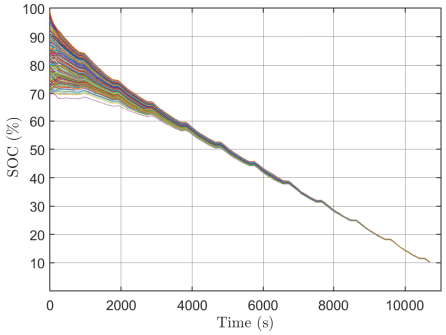

(b)

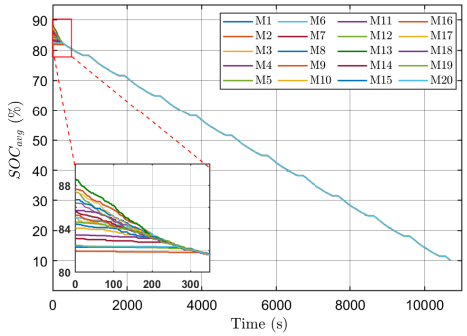

(c)

FIGURE 17. HIL system results using AF mission profile: (a) SOC of 320 cells with conventional system. (b) SOC of cells with proposed DRB system. (c) SOC of modules with proposed DRB system.

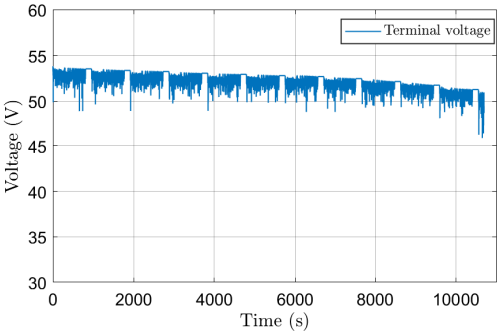

FIGURE 18. Terminal voltage of large scale pack with proposed system.

4. These performances demonstrate substantial potential for industrial vehicles, such as autonomous forklifts. Extended operational periods between charge cycles minimize the need for frequent recharging stops, thereby boosting overall productivity and mission capabilities. This highlights the DRB system's suitability not only for electric vehicles but also for demanding industrial environments where reliability, and energy efficiency are critical.

It's worth mentioning that the average execution time of the proposed algorithm, under the considered large scale battery, is around 0.3 s per iteration compared to 1.8 s for DRB System 1, making the proposed strategy nearly six times faster. This short time demonstrates the low computational complexity of the algorithm, which is particularly effective when it comes to managing cells as collective modules, rather than treating each cell individually. Such an approach considerably simplifies the computational requirements, making it an entirely feasible solution for optimizing the operation of large battery packs. Given the processing capabilities of modern battery management systems, this efficiency is expected to translate seamlessly into real-world applications, ensuring fast and reliable operation in practical environments.

E. DISCUSSION

- **Influence of weight parameters on optimization performance:**

To analyze the effect of the weight matrices $\alpha = [\alpha_1, \alpha_2, \alpha_3]$

and the switching penalty β on the optimization outcome, four test configurations were evaluated on a battery pack composed of 12 cells. All cases used the same initial SOC distribution but different weights, as presented in Table 5.

TABLE 5. Weight impact on equalization performance.

Case	$\alpha = [\alpha_1, \alpha_2, \alpha_3]$	β	P_{score}
1	[0.4, 0.1, 0.5]	0.1	0.885
2	[0.4, 0.1, 0.5]	0.5	0.780
3	[0.1, 0.4, 0.5]	0.1	0.835
4	[0.1, 0.4, 0.5]	0.5	0.765

α_3 was kept constant to respect load fulfillment constraint, which is essential for maintaining system functionality during reconfiguration. The overall system performance was quantified using a custom performance score defined as:

$$P_{\text{score}} = \omega_1 \left(1 - \frac{E_{\text{rem}}}{E_{\text{total}}}\right) + \omega_2 \left(1 - \frac{T_{\text{eq}}}{T_{\text{total}}}\right) + \omega_3 \left(1 - \frac{N_{\text{switch}}}{N_{\text{total}}}\right) \tag{20}$$

where E_{rem} represents the remaining energy at the end of discharge cycle, T_{eq} is the time required to reach inter-module SOC balance and N_{switch} is the number of switch activations during operation. $\omega_i, i = 1, .., 3$ represents the correspondent weights $\sum_{i=1}^{3} \omega_i = 1$. Fig.19 illustrates the impact of weight selection on SOC equalization behavior in Case 1 and Case 3.

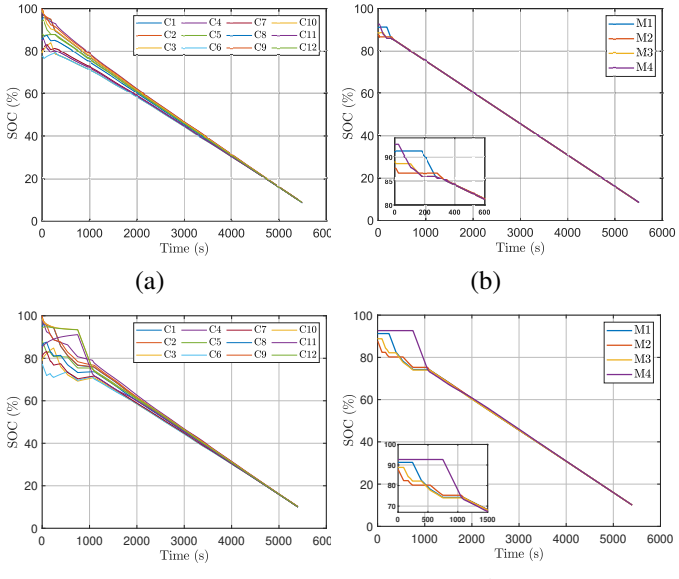

FIGURE 19. (a) and (b) SOC of cells and modules respectively of case1. (b) and (d) SOC of individual cells and modules respectively of case3.

As shown in Fig.19(a) and (b), where inter-module equalization is prioritized $\alpha_1 > \alpha_2$, SOC redistribution across modules occurs more rapidly. Module-level equalization is achieved in less than 400 seconds, and the system reaches a longer operational duration of 5450 seconds. This configuration leverages global balancing to improve energy distribution efficiency, and as inter-module balancing naturally triggers intra-module balancing, it accelerates total system equalization. In contrast, Fig.19(c) and (d) prioritizes intra-module equalization $\alpha_2 > \alpha_1$. In this case, modules are isolated more frequently, and their internal balancing persists for longer periods, leading to visible local SOC increases in some cells due to charge redistribution. While this strategy enhances uniformity within each module, it slows down the global balancing process, since prolonged idle phases may be required for cells to reach equilibrium. This extended isolation reduces overall efficiency, as the remaining modules continue operating without contributing to equalization. As a result, module-level equalization is delayed up to 1000 seconds, slightly reducing total operation time to 5398 seconds. This comparison highlights that emphasizing inter-module balancing not only accelerates system-wide SOC redistribution but also enhances energy usage and autonomy.

The effect of the switching penalty β is also critical to optimization performance, as shown in Table 5. A higher β, as in Case 2 and Case 4, imposes stricter switching constraints, leading to reduced reconfiguration flexibility and consequently poorer equalization performance. On the other hand, lower β, as in Case 1 and Case 3, allows for frequent switching, which improves equalization speed but may negatively affect system reliability and efficiency due to excessive module activations. Nevertheless, the optimization framework incorporates explicit constraints that limit unnecessary switching, ensuring that even under lower β, the number of activations remains within an acceptable range, preserving system efficiency.

A surface plot was generated as shown in Fig.20 to summarize the combined effect of α_2 and β on system performance, with α_3 fixed and α_1 adjusted accordingly. The plot highlights that the best performance is achieved when α_2 and β are both low, confirming that emphasizing inter-module equalization and maintaining reconfiguration flexibility leads to faster balancing and more efficient energy utilization.

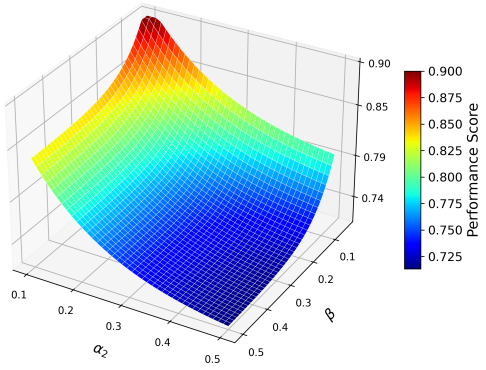

FIGURE 20. Impact of equalization weights and switching Penalty on performance.

- **Fault tolerance and switching-loss analysis:**

Switching devices play a critical role in both the safety and energy efficiency of reconfigurable battery systems. Potential failure modes, such as short circuits, overheating, or degradation under high current stress, are central concerns in battery design. The modular structure of the proposed DRB system inherently limits fault propagation by bypassing the affected module without impacting overall system operation. Moreover, the use of uniform switching commands at the module level, reduces the risk of control logic errors and unsafe switching scenarios compared to architectures requiring independent per-cell control. Beyond safety, switching components directly impact efficiency through their internal on-resistance R_{on}. To quantify this effect, an analytical evaluation was performed by varying R_{on} under a constant discharge current using a 3S4P battery configuration. Fig.21 presents the total energy delivered to the load and the corresponding losses as a function of R_{on}.

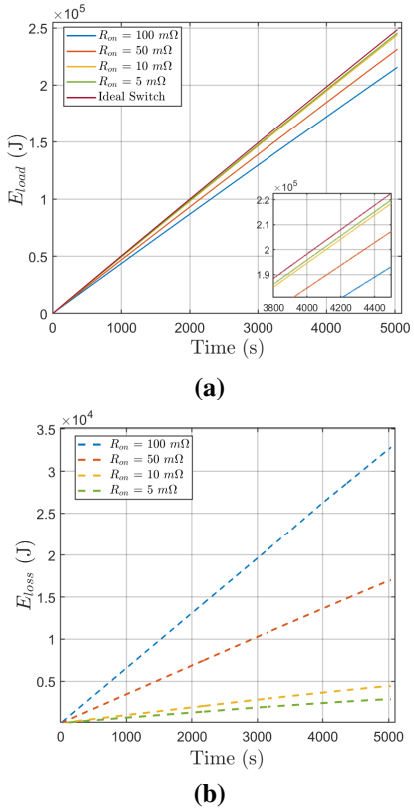

FIGURE 21. Impact of switch On-Resistance on: (a) Total energy delivered to the load and (b) Cumulative switching losses over time.

As shown in Fig.21, increasing switch resistances leads to significant reductions in delivered energy, compared to the ideal switch case—where R_{on} is assumed negligible. For instance, a high on-resistance results in an energy loss of approximately 6% of total energy, while lower R_{on} values (<50 mΩ), significantly improve energy efficiency with energy losses less than 2% of total energy. These results highlight the importance of selecting low-R_{on} switch devices, especially in high-current conditions. In the current prototype, mechanical relays were used to validate the proposed control strategy due to their simplicity and low cost. While suitable for proof-of-concept, their mechanical nature introduces long-term reliability concerns, which may become critical in large-scale implementations. The adoption of high-performance power switches, such as MOSFET is further recommended, as they are well-suited for real-world deployment due to their low R_{on}-resistance, high switching speed, and improved thermal performance. A transition toward MOSFETs is therefore planned in our future work. Specifically, we plan to replace the relays with two N-channel power MOSFETs connected in inverse series to minimize surge currents and ensure controlled bi-directional current flow [42]. Additionally, software-based diagnostic tools will be incorporated to monitor switch health, detect abnormal behaviors, and trigger safe reconfiguration actions under fault conditions [19, 75].

V. CONCLUSION

This paper introduced a reconfigurable battery system featuring a modular architecture with a dual-scale optimization control strategy designed to maximize capacity utilization and extend battery autonomy. By integrating a GA-based approach with a FNN predictive model, the proposed solution addresses computational challenges often associated with global optimization strategies. This integration enhances system efficiency and reliability through real-time closed-loop control, effectively balancing load demands and operational constraints. The major findings are summarized as follows:

- Experimental and HIL validations demonstrated the effectiveness of the proposed strategy in managing cell balancing under constant and dynamic load profiles. The DRB system improved energy utilization by 17% and extended operating time by 18%, compared to conventional systems, demonstrating its ability to optimize battery performance under controlled conditions.
- Scalability tests conducted on a large-scale battery pack consisting of 320 cells highlighted the DRB system's potential for real-world applications, such as autonomous vehicles. Battery autonomy improvements of up to 29% were observed, proving the system's capability to handle complex configurations while maintaining reliability and efficiency.
- The modular architecture and GA-based control strategy significantly reduce computational complexity by focusing on module-level management rather than individual cells. This approach ensures efficient equalization between and within modules, minimizes operational costs, and guarantees system safety by maintaining a minimum number of active modules connected to the load at all times.

Future work will focus on enhancing the control strategy by extending the prediction horizon to enable more accurate anticipation of power demand. To ensure long-term robustness under realistic conditions, the predictive model will be

further refined by incorporating aging effects such as cell degradation, thermal behavior, and resistance growth. Additionally, the sensitivity of the control strategy to parameter variations will be systematically investigated to assess its resilience and ensure reliable performance. Experimental developments are also planned to support the expansion toward larger-scale physical validation.

ACKNOWLEDGMENT

This work was supported by the Industrial Research Chair Noovelia and by the Natural Science and Engineering Research Council of Canada.

DECLARATION OF AI-ASSISTED TECHNOLOGIES IN THE WRITING PROCESS

During the preparation of this work, the corresponding author used ChatGPT in order to improve the language and readability of the manuscript. After using this tool/service, the authors reviewed and edited the content as needed and take full responsibility for the content of the publication.

REFERENCES

[1] S. Sarmah, Lakhanlal, B. K. Kakati, D. Deka, Recent advancement in rechargeable battery technologies, WIREs Energy and Environment 12 (2023) e461.

[2] T. Baumhöfer, M. Brühl, S. Rothgang, D. U. Sauer, Production caused variation in capacity aging trend and correlation to initial cell performance, Journal of Power Sources 247 (2014) 332–338.

[3] L. Y. Wang, G. Yin, Y. Ding, C. Zhang, State of health based battery reconfiguration for improved energy efficiency, Control Theory and Technology 20 (2022) 443–455.

[4] S. Santhanagopalan, R. E. White, Quantifying cell-to-cell variations in lithium ion batteries, International Journal of Electrochemistry 2012 (2012) 395838.

[5] K. Kim, J.-I. Choi, Effect of cell-to-cell variation and module configuration on the performance of lithium-ion battery systems, Applied Energy 352 (2023) 121888.

[6] S. F. Schuster, M. J. Brand, P. Berg, M. Gleissenberger, A. Jossen, Lithium-ion cell-to-cell variation during battery electric vehicle operation, Journal of Power Sources 297 (2015) 242–251.

[7] Y. Hua, S. Zhou, H. Cui, X. Liu, C. Zhang, X. Xu, H. Ling, S. Yang, A comprehensive review on inconsistency and equalization technology of lithium-ion battery for electric vehicles, International Journal of Energy Research 44 (2020) 11059–11087.

[8] N. Ghaeminezhad, Q. Ouyang, X. Hu, G. Xu, Z. Wang, Active cell equalization topologies analysis for battery packs: A systematic review, IEEE Transactions on Power Electronics 36 (2021) 9119–9135.

[9] S. Kıvrak, T. Özer, Y. Oğuz, E. B. Erken, Battery management system implementation with the passive control method using mosfet as a load, Measurement and Control 53 (2020) 205–213.

[10] J. Carter, Z. Fan, J. Cao, Cell equalisation circuits: A review, Journal of Power Sources 448 (2020) 227489.

[11] F. Feng, X. Hu, J. Liu, X. Lin, B. Liu, A review of equalization strategies for series battery packs: variables, objectives, and algorithms, Renewable and Sustainable Energy Reviews 116 (2019) 109464.

[12] W. Han, T. Wik, A. Kersten, G. Dong, C. Zou, Next-generation battery management systems: Dynamic reconfiguration, IEEE Industrial Electronics Magazine 14 (2020) 20–31.

[13] L. Komsiyska, T. Buchberger, S. Diehl, M. Ehrensberger, C. Hanzl, C. Hartmann, M. Hölzle, J. Kleiner, M. Lewerenz, B. Liebhart, et al., Critical review of intelligent battery systems: Challenges, implementation, and potential for electric vehicles, Energies 14 (2021) 5989.

[14] Z. Wei, J. Zhao, H. He, G. Ding, H. Cui, L. Liu, Future smart battery and management: Advanced sensing from external to embedded multi-dimensional measurement, Journal of Power Sources 489 (2021) 229462.

[15] T. Kacetl, J. Kacetl, N. Tashakor, S. Goetz, Ageing mitigation and loss control in reconfigurable batteries in series-level setups, in: 2022 24th European Conference on Power Electronics and Applications (EPE'22 ECCE Europe), 2022, pp. 1–11.

[16] R. Thomas, F. Lehmann, J. Blatter, G. Despesse, V. Heiries, Performance analysis of a novel high frequency self-reconfigurable battery, World Electric Vehicle Journal 12 (2021) 10.

[17] Z. Zhao, J. Xu, Z. Liu, X. Zhang, X. Mei, Reconfigurable battery system-based hybrid self-heating method for low temperature applications, IEEE Transactions on Industrial Informatics 20 (2024) 12826–12836.

[18] M. Schmid, E. Gebauer, C. Endisch, Structural analysis in reconfigurable battery systems for active fault diagnosis, IEEE Transactions on Power Electronics 36 (2021) 8672–8684.

[19] H. Xu, L. Cheng, D. Paizulamu, H. Zheng, Safety and reliability analysis of reconfigurable battery energy storage system, Batteries 11 (2024) 12.

[20] N. Bouchhima, M. Schnierle, S. Schulte, K. P. Birke, Optimal energy management strategy for self-reconfigurable batteries, Energy 122 (2017) 560–569.

[21] D. Karunathilake, M. Vilathgamuwa, Y. Mishra, P. Corry, T. Farrell, S. S. Choi, Degradation-conscious multiobjective optimal control of reconfigurable li-ion battery energy storage systems, Batteries 9 (2023) 217.

[22] A. Wiedenmann, J. Buberger, T. Högerl, W. Grupp, M. Hohenegger, M. Kuder, T. Weyh, A. Neve, Proactive balancing for reconfigurable battery systems with automated efficiency analysis, in: 2023 International Conference on Smart Energy Systems and Technologies (SEST), 2023, pp. 1–6.

[23] N. Bouchhima, M. Gossen, S. Schulte, K. P. Birke, Lifetime of self-reconfigurable batteries compared with conventional batteries, Journal of Energy Storage 15

(2018) 400–407.

[24] J. Blatter, V. Heiries, R. Thomas, G. Despesse, Optimal lifetime management strategy for self-reconfigurable batteries, in: 2022 IEEE 95th Vehicular Technology Conference: (VTC2022-Spring), 2022, pp. 1–7.

[25] A. Škegro, C. Zou, T. Wik, Analysis of potential lifetime extension through dynamic battery reconfiguration, in: 2023 25th European Conference on Power Electronics and Applications (EPE'23 ECCE Europe), 2023, pp. 1–11.

[26] S. Muhammad, M. U. Rafique, S. Li, Z. Shao, Q. Wang, X. Liu, Reconfigurable battery systems: A survey on hardware architecture and research challenges, ACM Transactions on Design Automation of Electronic Systems (TODAES) 24 (2019) 1–27.

[27] S. Jeon, J. Kim, J. Ahn, H. Cha, Optimizing discharge efficiency of reconfigurable battery with deep reinforcement learning, IEEE Transactions on Computer-Aided Design of Integrated Circuits and Systems 39 (2020) 3893–3905.

[28] B. Y.K., A. V.P., V. U., P. G.K., Single-port and multi-port self-reconfigurable battery topologies for dynamic cell balancing, Journal of Energy Storage 119 (2025) 116402.

[29] A. Mondoha, J. Sabatier, P. Lanusse, S. Tippmann, C. Farges, Nonlinear model predictive control for a simulated reconfigurable battery pack, IFAC-PapersOnLine 54 (2021) 353–358. 7th IFAC Conference on Nonlinear Model Predictive Control NMPC 2021.

[30] H. Zhang, Y. Wang, H. Qi, J. Zhang, Active battery equalization method based on redundant battery for electric vehicles, IEEE Transactions on Vehicular Technology 68 (2019) 7531–7543.

[31] F. Yang, F. Gao, B. Liu, S. Ci, An adaptive control framework for dynamically reconfigurable battery systems based on deep reinforcement learning, IEEE Transactions on Industrial Electronics 69 (2022) 12980–12987.

[32] Z. Wei, H. Cui, X. Liu, Y. Li, R. Wang, Real-time reconfiguration-based all-cell flexibility and capacity maximum utilization of second- life batteries, IEEE Transactions on Transportation Electrification 11 (2025) 1035–1047.

[33] F. Ji, L. Liao, T. Wu, C. Chang, M. Wang, Self-reconfiguration batteries with stable voltage during the full cycle without the dc-dc converter, Journal of Energy Storage 28 (2020) 101213.

[34] Y.-Y. Chou, C.-W. Wu, M.-D. Shieh, C.-H. Chen, Battery pack reliability and endurance enhancement for electric vehicles by dynamic reconfiguration, in: 2022 IEEE 31st Asian Test Symposium (ATS), 2022, pp. 66–71.

[35] J. Blatter, V. Heiries, R. Thomas, G. Despesse, Nonlinear model predictive control for lifetime extension of self-reconfigurable batteries, in: SSI 2022 - Smart Systems Integration, IEEE, 2022.

[36] L. He, E. Kim, K. G. Shin, A case study on improving capacity delivery of battery packs via reconfiguration, ACM Transactions on Cyber-Physical Systems 1 (2017) 1–23.

[37] S. Baccari, M. Tipaldi, V. Mariani, Deep reinforcement learning for cell balancing in electric vehicles with dynamic reconfigurable batteries, IEEE Transactions on Intelligent Vehicles 9 (2024) 6450–6461.

[38] Y. Weng, C. Ababei, Ai-assisted reconfiguration of battery packs for cell balancing to extend driving runtime, Journal of Energy Storage 84 (2024) 110853.

[39] D. Karnehm, W. Bliemetsrieder, S. Pohlmann, A. Neve, Controlling algorithm of reconfigurable battery for state of charge balancing using amortized q-learning, Batteries 10 (2024) 131.

[40] X. Yang, P. Liu, F. Liu, Z. Liu, D. Wang, J. Zhu, T. Wei, A dod-soh balancing control method for dynamic reconfigurable battery systems based on dqn algorithm, Frontiers in Energy Research 11 (2023) 1333147.

[41] H. Cui, Z. Wei, H. He, J. Li, Novel reconfigurable topology-enabled hierarchical equalization of lithium-ion battery for maximum capacity utilization, IEEE Transactions on Industrial Electronics 70 (2023) 396–406.

[42] S.-Z. Chen, Y. Wang, G. Zhang, L. Chang, Y. Zhang, Sneak circuit theory based approach to avoiding short-circuit paths in reconfigurable battery systems, IEEE Transactions on Industrial Electronics 68 (2021) 12353–12363.

[43] Y. Li, P. Yin, J. Chen, Active equalization of lithium-ion battery based on reconfigurable topology, Applied Sciences 13 (2023) 1154.

[44] A. Farakhor, D. Wu, Y. Wang, H. Fang, A novel modular, reconfigurable battery energy storage system: Design, control, and experimentation, IEEE Transactions on Transportation Electrification 9 (2023) 2878–2890.

[45] M. Uzair, G. Abbas, S. Hosain, Characteristics of battery management systems of electric vehicles with consideration of the active and passive cell balancing process, World Electric Vehicle Journal 12 (2021) 120.

[46] Z. B. Omariba, L. Zhang, D. Sun, Review of battery cell balancing methodologies for optimizing battery pack performance in electric vehicles, IEEE Access 7 (2019) 129335–129352.

[47] M. Kauer, S. Narayanaswamy, S. Steinhorst, S. Chakraborty, Rapid analysis of active cell balancing circuits, IEEE Transactions on Computer-Aided Design of Integrated Circuits and Systems 36 (2017) 694–698.

[48] J. Tian, Q. Zhang, X. Liu, Y. Fan, Y. Wang, T. Pan, Route planning-based active equalization of reconfigurable battery packs in electric vehicles, IEEE Transactions on Intelligent Vehicles 9 (2024) 6524–6537.

[49] Z. Chen, C. Liu, Y. Zhang, R. Yang, G. Chen, Hierar-

chical state-of-charge balancing and second-harmonic current suppressing control with a scalable dc reconfigurable battery pack, IEEE Transactions on Power Electronics 39 (2024) 6758–6768.
[50] J. Dang, D. Xiao, X. Zhang, R. Jia, Y. Jiao, Optimal configuration of retired battery reconfigurable network considering switching losses, Journal of Energy Storage 101 (2024) 113735.
[51] L. He, L. Kong, Y. Gu, C. Liu, T. He, K. G. Shin, Extending battery system operation via adaptive reconfiguration, ACM Transactions on Sensor Networks (TOSN) 15 (2019) 1–21.
[52] G. Cârstoiu, M. V. Micea, L. Ungurean, M. Marcu, Novel battery wear leveling method for large-scale reconfigurable battery packs, International Journal of Energy Research 45 (2021) 1932–1947.
[53] S. L. Gorantla, B. Bose, W. Li, A. Garg, L. Gao, B. Babu, A novel feedback control algorithm for effective design of reconfigurable battery packs for electric vehicles, Sustainable Energy, Grids and Networks 38 (2024) 101287.
[54] M.-K. Tran, M. Mathew, S. Janhunen, S. Panchal, K. Raahemifar, R. Fraser, M. Fowler, A comprehensive equivalent circuit model for lithium-ion batteries, incorporating the effects of state of health, state of charge, and temperature on model parameters, Journal of Energy Storage 43 (2021) 103252.
[55] X. Lai, Y. Zheng, T. Sun, A comparative study of different equivalent circuit models for estimating state-of-charge of lithium-ion batteries, Electrochimica Acta 259 (2018) 566–577.
[56] X. Hu, S. Li, H. Peng, A comparative study of equivalent circuit models for li-ion batteries, Journal of Power Sources 198 (2012) 359–367.
[57] M. Kim, E. Kang, S. Lee, M. Song, B. Ko, J. Lee, W. Na, J. Kim, Weighted model-based state-of-charge estimation algorithm for differential terminal voltage application of lfp battery, in: 2024 IEEE Energy Conversion Congress and Exposition (ECCE), 2024, pp. 1779–1783.
[58] B. Zine, H. Bia, A. Benmouna, M. Becherif, M. Iqbal, Experimentally validated coulomb counting method for battery state-of-charge estimation under variable current profiles, Energies 15 (2022) 8172.
[59] A. Maragur, S. Prem, A. G. Hagargund, M. Gangadharaih, V. Devara, State-of-charge approximation using coulomb counting for lithium ion batteries – a low-cost approach, in: 2024 International Conference on Vehicular Technology and Transportation Systems (ICVTTS), volume 1, 2024, pp. 1–5.
[60] N. Lin, S. Ci, D. Wu, A novel low-cost online state of charge estimation method for reconfigurable battery pack, in: 2016 IEEE Applied Power Electronics Conference and Exposition (APEC), 2016, pp. 3189–3192.
[61] W. Han, A. Kersten, Analysis and estimation of the maximum circulating current during the parallel operation of reconfigurable battery systems, in: 2020 IEEE Transportation Electrification Conference Expo (ITEC), 2020, pp. 229–234.
[62] R. Xiong, J. Cao, Q. Yu, H. He, F. Sun, Critical review on the battery state of charge estimation methods for electric vehicles, IEEE Access 6 (2018) 1832–1843.
[63] T. A. Fagundes, G. H. F. Fuzato, L. J. R. Silva, A. M. d. S. Alonso, J. C. Vasquez, J. M. Guerrero, R. Q. Machado, Battery energy storage systems in microgrids: A review of soc balancing and perspectives, IEEE Open Journal of the Industrial Electronics SOCiety 5 (2024) 961–992.
[64] Z. Fu, B. Sun, J. Gong, M. Gong, X. Zhao, S. Ma, A soc estimation method for li-ion batteries under high-rate pulse conditions based on ao-bpnn model, Space: Science & Technology 3 (2023) 0088.
[65] M. H. Sulaiman, Z. Mustaffa, State of charge estimation for electric vehicles using random forest, Green Energy and Intelligent Transportation 3 (2024) 100177.
[66] O. Ali, M. K. Ishak, F. Memon, M. S. M. Asaari, Estimation of battery state-of-charge using feedforward neural networks, in: 2022 19th International Conference on Electrical Engineering/Electronics, Computer, Telecommunications and Information Technology (ECTI-CON), 2022, pp. 1–4.
[67] Z. Cui, L. Wang, Q. Li, K. Wang, A comprehensive review on the state of charge estimation for lithium-ion battery based on neural network, International Journal of Energy Research 46 (2022) 5423–5440.
[68] T. Wasanapradit, N. Mukdasanit, N. Chaiyaratana, T. Srinophakun, Solving mixed-integer nonlinear programming problems using improved genetic algorithms, Korean Journal of Chemical Engineering 28 (2011) 32–40.
[69] S. Jinlei, L. Wei, T. Chuanyu, W. Tianru, J. Tao, T. Yong, A novel active equalization method for series-connected battery packs based on clustering analysis with genetic algorithm, IEEE Transactions on Power Electronics 36 (2021) 7853–7865.
[70] C. H. Ricardo, L. H. Adriana, D. A. Nelson, Energy management supported on genetic algorithms for the equalization of battery energy storage systems in microgrid systems, Journal of Energy Storage 72 (2023) 108510.
[71] X. Zhang, J. Lei, H. Li, Z. Yu, Z. Huang, J. Peng, Digital twin driven reconfiguration of li-ion batteries with capacity delivery maximization, in: 2022 IEEE Industry Applications SOCiety Annual Meeting (IAS), 2022, pp. 1–9.
[72] C. Patel, Developing battery management systems using simulink, in: MATLAB EXPO, 2019. Accessed: Jan. 24, 2024. [Online]. Available : www.matlabexpo.com.
[73] M. Tutuianu, P. Bonnel, B. Ciuffo, T. Haniu, N. Ichikawa, A. Marotta, J. Pavlovic, H. Steven, Development of the world-wide harmonized light duty test

cycle (wltc) and a possible pathway for its introduction in the european legislation, Transportation Research Part D: Transport and Environment 40 (2015) 61–75.

[74] M. Mohammadpour, S. Kelouwani, M.-A. Gaudreau, L. Zeghmi, A. Amamou, H. Bahmanabadi, B. Allani, M. Graba, Energy-efficient motion planning of an autonomous forklift using deep neural networks and kinetic model, Expert Systems with Applications 237 (2024) 121623.

[75] Y. Chen, E. Lin, Y. Zhou, Q. Yu, S. Ci, Y. Zhuang, Transient analysis in dynamic reconfigurable battery system, in: 2022 IEEE International Conference on Power Systems Technology (POWERCON), 2022, pp. 1–6.

GHADA BEN DEBBA received the B.S. degree in Industrial Computing and Automatic Science from the National Institute of Applied Sciences and Technology, Tunis, Tunisia, in 2022, and the M.S. degree in Information Systems Techniques from the National Engineering School of Tunis, Tunisia, in 2022. She is currently pursuing the Ph.D. degree in electrical and computer engineering at the University of Quebec at Trois-Rivières (UQTR), Quebec, Canada. Her current research focuses on battery management systems, energy optimization, and real-time control strategies for reconfigurable battery architectures, with applications in electric vehicles and smart manufacturing.

ALI AMAMOU (Member, IEEE) received the B.S. degree in Industrial Computing and Automatic Science from the National Institute of Applied Sciences and Technology, Tunis, Tunisia, in 2013, and the M.S. degree in Embedded Systems Science from Arts et Métiers ParisTech University, France, in 2014. Between 2015 and 2018, he completed his Ph.D. in energy and thermal management of electric vehicles in cold weather conditions at the University of Quebec at Trois-Rivières (UQTR), Quebec, Canada. He is currently an Associate Professor at UQTR, where he also serves as a project lead for several industrial collaborations focused on smart manufacturing and energy-efficient systems. His research combines energy systems and robotics through the development of intelligent, energy-efficient autonomous systems. His work focuses on the modeling, optimization, and control of hybrid energy systems for electric and hydrogen-powered vehicles, with the goal of efficiently powering onboard systems while maximizing vehicle autonomy and energy performance. By integrating hybrid and hydrogen-based energy sources with robotic platforms, he contributes to the advancement of autonomous navigation, eco-energy planning, and smart control in both vehicular and industrial contexts. He actively collaborates with industrial partners to transfer innovative, sustainable technologies into practice.

SOUSSO KELOUWANI (Senior Member, IEEE) received the Ph.D. degree in robotics systems from the Ecole Polytechnique de Montreal, in 2011. He completed his Postdoctoral Internship on fuel cell hybrid electric vehicles with the University of Quebec at Trois-Rivières (UQTR), in 2012. He developed expertise in the optimization and intelligent control of vehicular applications. He has been a Full Professor of Mechatronics with the Department of Mechanical Engineering, since 2017, and a member of the Hydrogen Research Institute. He holds four patents in U.S. and Canada. He has published more than 100 scientific articles. His research interests include optimizing energy systems for vehicle applications, advanced driver assistance techniques, and intelligent vehicle navigation taking into account Canadian climatic conditions.

Holder of the Canada Research Chair in Energy Optimization of Intelligent Transport Systems and holder of the Noovelia Research Chair in Intelligent Navigation of Autonomous Industrial Vehicles. Prof. Kelouwani was co-president and president of the technical committee of the IEEE International Conferences on Vehicular Power and Propulsion in Chicago (USA, 2018) and in Hanoi (Vietnam, 2019). He is the winner of the Canada General Governor Gold Medal, in 2003, and a member of the Order of Engineers of Quebec. In 2019, his team received the First Innovation Prize in partnership with Noovelia, awarded by the Association des Manufacturiers de la Mauricie et Center-du-Quebec for the development of an autonomous and natural navigation system. In 2017, he received the Environment Prize from the Gala des Grands Prix d'excellence en transport, the Association quebecoise du Transport (AQTr), for the development of hydrogen range extenders for electric vehicles.

NAIMA SEHLI received the B.S. degree in Industrial Computing and Automatic Science from the National Institute of Applied Sciences and Technology, Tunis, Tunisia, in 2016. She successfully defended her PhD thesis in 2022, completed under joint supervision between the National Engineering School of Tunis, Tunisia, and the Conservatoire National des Arts et Métiers, France. Since 2022, Dr. Sehli has been engaged as a postdoctoral researcher at the Hydrogen Research Institute of the University of Québec at Trois-Rivières, Canada. Her research focuses primarily on the modeling and electrical simulation of hydrogen fuel cells.